Mahdi and El Abbadi *Iraqi Journal of Science, 2022, Vol. 63, No. 9, pp: 4022-4046*
DOI: 10.24996/ijs.2022.63.9.32

ISSN: 0067-2904

Glaucoma Diagnosis Based on Retinal Fundus Image: A Review

Hussein Mahdi *, Nidhal El Abbadi
Department of Computer Science, College of Computer Science and Mathematics,University of Kufa, Najaf, Iraq

Received: 27/9/2021 Accepted: 9/12/2021 Published: 30/9/2022

Abstract

Glaucoma is one of the most dangerous eye diseases. It occurs as a result of an imbalance in the drainage and flow of the retinal fluid. Consequently, intraocular pressure is generated, which is a significant risk factor for glaucoma. Intraocular pressure causes progressive damage to the optic nerve head, thus leading to vision loss in the advanced stages. Glaucoma does not give any signs of disease in the early stages, so it is called "the Silent Thief of Sight". Therefore, early diagnosis and treatment of retinal eye disease is extremely important to prevent vision loss. Many articles aim to analyze fundus retinal images and diagnose glaucoma. This review can be used as a guideline to help diagnose glaucoma. It presents 63 articles related to the applications of fundus retinal analysis. Applications of the glaucomatous image classification are improving fundus images by locating and segmenting the optic disc, optic cup, fovea, and blood vessels. The study also presents datasets, metrics, and parameters that indicate the changes in retina structure and the steps and results for each paper.

Keywords: Retinal Fundus Image, Glaucoma Screening, Cup-Disc-Ratio (CDR), Optic Nerve Head (ONH), Joint Segmentation Optic Disc and Optic Cup.

دراسة في تشخيص مرض الكلوكوما بالاعتماد على صورة قاع الشبكية

حسين مهدي*, نضال العبادي
قسم علوم الحاسبات, كلية علوم الحاسبات والرياضيات, جامعة الكوفة, النجف, العراق

الخلاصة

الكلوكوما (الماء الاسود او الماء الازرق) احد اخطر امراض العين. يحدث نتيجة خلل في تصريف وتدفق سائل الشبكية. و بالتالي يتولد ضغط داخل العين. و هو عامل خطورة مهم للإصابة بالكلوكوما. يتسبب الضغط داخل العين في تلف تدريجي لرأس العصب البصري ، مما يؤدي إلى فقدان البصر في المراحل المتقدمة. لا يعطي الجلوكوما أي علامات للمرض في المراحل المبكرة ، لهذا يطلق عليه "سارق البصر الصامت" لذلك فإن التشخيص المبكر وعلاج أمراض الشبكية أمر بالغ الأهمية لمنع فقدان البصر. تهدف العديد من المقالات إلى تحليل صور شبكية قاع العين لتشخيص الكلوكوما. بالإمكان استعمال هذه الدراسة كدليل ارشادي يساعد في تشخيص مرض الكلوكوما. تعرض الدراسة (63) بحث يتعلق بتطبيقات تحليل قاع

*Email: husseinmahdiali@yahoo.com

الشبكية. المفاهيم الاساسية او تطبيقات تصنيف صور الكلوكوما هي في تحسين صور قاع العين، تحديد و تقسيم القرص البصري، والكأس البصري، والنقرة، والأوعية الدموية. تعرض الدراسة أيضًا قواعد البيانات، مقاييس الاداء، المعايير التي تشير إلى التغييرات في بنية شبكية العين، كذلك خطوات ونتائج كل مقالة.

1. Introduction

According to the World Health Organization (WHO), the number of people suffering from glaucoma is estimated at 64 million in 2016 [1], 80 million in 2020 [2], and this number will increase to 95 million by 2030 [1], and 110 million by 2040 [3]. It is worth mentioning that glaucoma disease is responsible for about 12% of all people who lose their sight [3]. Therefore, glaucoma is considered the second leading cause of blindness in the world [4]. The large numbers of diseases are caused by the fact that glaucoma is a silent disease, and the disease can only be identified after an increase in the intraocular pressure (due to disorder in the flow of the eye fluid system) and destruction of some cells of the optic nerve. This is in the early stages. Generally, a person with glaucoma has several conditions such as increasing the intraocular pressure (IOP), damaging the optic nerve head (ONH), and losing the visual field [1].

For the reasons above, it is necessary to detect glaucoma at an early stage because glaucoma disease is a severe disorder. The damage it causes is irremediable. It leads to perpetual loss of sight if not cured promptly. There are no perceptible indications in its preliminary stages. There is no prophylactic treatment for glaucoma. Analyzing the optic nerve head is the essential and critical factor in diagnosing glaucoma in the early stages [5].

In recent years, computer-aided diagnosis (CAD) systems based on medical images have been in increasing demand since the retina is the visible portion of the nervous system that connects directly to the brain. A retina provides vital information and features for diagnosing several eye diseases, including cataracts, glaucoma, diabetic retinopathy, and age-related macular degeneration. This information and characteristics are the color, size, and shape of parts or regions of the retina, such as Optic Disc, Optic Cup, Blood Vessels, Neuroretinal Rim, and Fovea [2]. Figure 1 shows the regions of the retinal fundus image.

This paper presents a comprehensive review of a collection of recent articles (Figure 2). The period covered by the published articles was from 2016 to 2021. These articles are considered noteworthy for our review. The review was based on the academic databases used to collect the articles, such as PubMed, Springer, Scopus, Google Scholar, IEEE Xplore, Science Direct, and Web of Science. Sections of the study provide guidelines to help researchers understand ophthalmic applications such as retinal fundus image enhancement, segmentation, and classification.

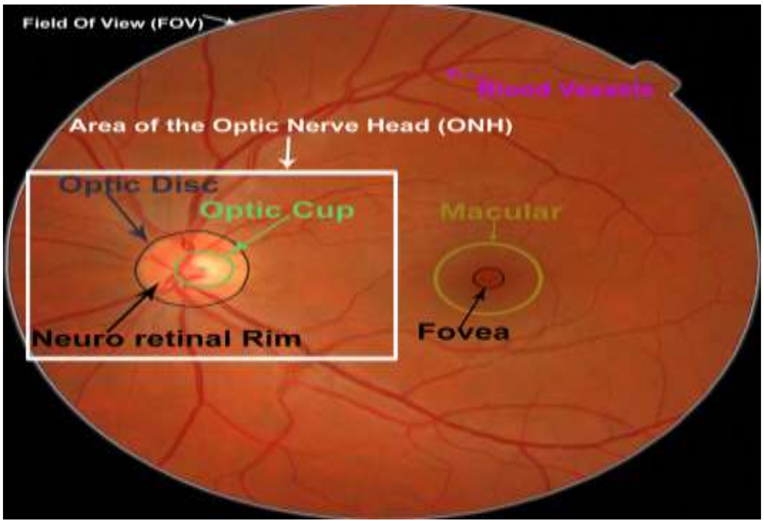

Figure 1-Structures of the retina fundus image.

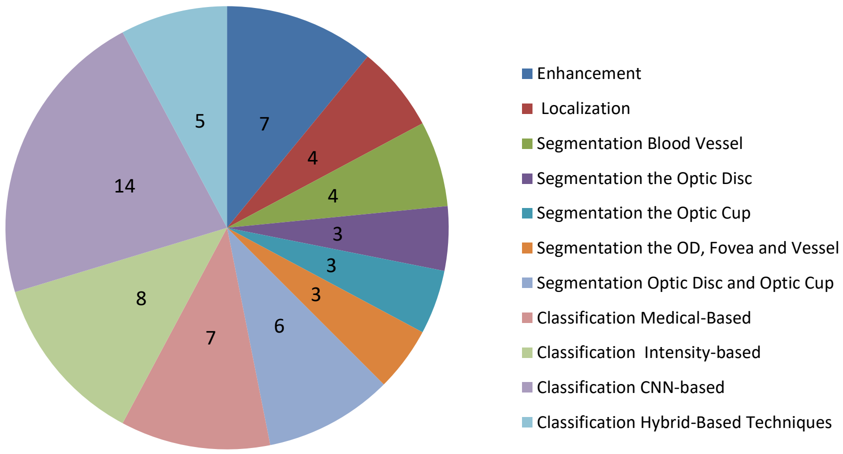

Figure 2-Category of articles per application.

2. Parameters Analysis

In glaucoma, intraocular pressure (IOP) causes several changes in the retina of the eye, especially in the area of the optic nerve head (ONH). Changes influence the level of vision because the ganglion cell axons pass through ONH to transmit images from the eye to the brain. Most retinal regions in Figure 1 are affected by these changes [6]. One of the most significant changes in glaucoma is the deformity that occurs in the optic disc (OD) and optic cup (OC) regions .This change leads to the occurrence of what is called "cupping," where the OD size increases and the thickness of the neuroretinal rim (NRR) decreases. Several parameters (structural indications) detect these changes and help to diagnose the glaucomatous image. For example, the Cup-to-Disc Ratio (CDR) parameter and the SNT rule recognize cupping [7]. Table 1 shows a set of parameters that are used to distinguish between healthy and glaucomatous images.

Table 1-Set of parameters analysis

Parameters	Abbreviation	Formula	Description
Vertical Diameter Cup to Disc Ratio [8]	CDR / VCDR	$\frac{Vertical\ Cup\ Diameter\ (VCD)}{Vertical\ Disc\ Diameter\ (VDD)}$	The ratio of the vertical diameter of the OC to the vertical diameter of the OD
Horizontal Diameter Cup to Disc Ratio [9]	HCDR	$\frac{Horizontal\ Cup\ Diameter\ (HCD)}{Horizontal\ Disc\ Diameter\ (HDD)}$	The ratio of the horizontal diameter of the OC to the horizontal diameter OD
Horizontal to Vertical CDR [8]	H-V CDR	$\frac{Horizontal\ CDR}{Vertical\ CDR}$	The ratio of the horizontal CDR to the vertical CDR
Cup to Disc Area Ratio [9]	CDAR	$\frac{Cup\ Area}{Disc\ Area}$	The ratio of the area of the OC to the area of the OD
Rim to Disc Area Ratio [10]	RDAR	$\frac{Rim\ Area}{Disc\ Area} = \frac{Aree(Disc - Cup)}{Aree(Disc)}$	The ratio of the area of the Neuroretinal Rim" (NRR) to the area of the OD
Rim to Disc Ratio [11]	RDR	$\frac{vertical\ neuro\ retinal\ rim(VNRR}{Vertical\ Disc\ Diameter\ (VDD)}$	The ratio of the VNRR (thickness of superior part only) to the vertical diameter of the OD
Rim Area Ratio [2]	RAR	$\frac{InferiorArea\ +\ Superior\ Area}{Nasal\ Area\ \ +Temporal\ Area}$	RAR is determined by removing the optical cup from the area of the optic disc.
Inferior, Superior, Nasal, and Temporal Rule [12]	ISNT Rule	Inferior> Superior> Nasal> Temporal	Healthy must keep the relation among the regions in descending order

Cup shape /Hausdorff's fractal dimension [11]	HFD	$HFD = \lim_{\epsilon \to 0} \frac{\log N(\epsilon)}{\log \epsilon^{-1}}$	N(ϵ) represents the number of hyper-cubes that fills the object with Euclidean dimension and length ϵ
Disc damage likelihood scale [9]	DDLS	$\frac{Mimum\ width\ of\ Rim}{Disc\ Diameter}$	The severity of Glaucoma is calculated by DDLS.
Glaucoma Risk Index [13]	GRI	GRI = 6.8375 - 1.1325 (PC1) - 1.6500 (PC2) + 2.7225 (PC3) + 0.6750 (PC4) + 0.6650 (PC5)	PCA (Principal Component analysis) healthy: GRI =(8.68 ± 1.67) Glaucomatous: GRI =(4.84 ± 2.08)

3. Retinal Fundus Image Datasets

There are some types of images used to diagnose diseases: Optical Coherence Tomography (OCT), Heidelberg Retinal Tomography (HRT), and Retinal Fundus Image (RFI). OCT and HRT are three-dimensional images. Unfortunately, these images are not widely available. The unavailability comes for two reasons. First, the devices used to capture images are expensive. Second, the devices require specialists to work on them [14]. However, retinal fundus images are two-dimensional images, which are widespread, and databases of these kinds of retinal images are available to researchers and specialists because of the low cost of the devices for capturing images and their presence in most ophthalmology centers. There are several datasets for RFI. The datasets are either public or private. For the reasons listed above, this study's focus on public datasets for RFI is due to the availability of datasets online. Researchers can make efficient comparisons between them, so researchers can benefit from them in their work. Table 2 shows the set of available datasets. Some existing datasets have been updated and have more than one version. This research referred to the number of images used in each article for each dataset because some researchers used just a part of the dataset or just a few images from the dataset.

Table 2-Widely used available datasets.

Dataset	Total	Glaucomatous	Normal	Information of Ground Truth	Link
ACRIMA [15]	705	396	309	Classification of normal and glaucomatous	https://figshare.com/s/c2d31f850af14c5b5232
HARVARD [16]	1542	756	786	Classification of normal and glaucomatous	https://dataverse.harvard.edu/dataset.xhtml?persistentId=doi:10.7910/DVN/1YRRAC
ORIGA [17]	650	168	482	Classification of normal and glaucomatous	https://github.com/Barcelona-Technology- School/InnoSpark-edir/tree/main/Datasets/ORIGA/glaucoma
sjchoi86-HRF [18]	401	101	300	Classification of normal and glaucomatous	https://github.com/yiweichen04/retina_dataset
JSIEC /kaggle [19]	51	13	38	Classification of normal and glaucomatous	https://www.kaggle.com/linchundan
GlaucomaDB [11], [20]	100	48	52	Classification of normal and glaucomatous	http://biomisa.org/index.php/glaucoma-database/
REFUGE-1 [21]	1200	120	1080	• Classification images • Segmentation for OC and OD • Location of Fovea	https://refuge.grand-challenge.org/Download/
REFUGE-2 [21]	1600	160	1440	• Classification images • Segmentation for OC and OD • Location of Fovea	https://refuge.grand-challenge.org/REFUGE2Download/
LAG [22]	5824	2392	3432	• Classification images • Attention maps	https://github.com/smilell/AG-CNN

DRISHTI-GS1 [23]	101	70	31	● Classification images ● Soft matt segmenting cup and disc ●CDR values and Disc center	http://cvit.iiit.ac.in/projects/mip/drishti-gs/mip-dataset2/enter.php
HRF [24]	45	15	15	● Classification images ● Segmentation Vessel and FOV ●Center and Radius for OD	https://www5.cs.fau.de/research/data/fundus-images/
RIM-ONE-r1 [25]	169	51	118	● Classification images ● Segmentations optic disc	http://medimrg.webs.ull.es/research/reitnal-imaging/rim-one/
RIM-ONE-r2 [25]	455	200	255	●Classification of images into normal and glaucomatous	http://medimrg.webs.ull.es/research/retinal-imaging/rim-one/
RIM-ONE-r3 [26]	159	74	85	● Classification images ● Segmentations of Cup and disc	http://medimrg.webs.ull.es/rim-one-release-3-is-finally-here/
RIM-ONE-DL [27]	485	172	313	● Classification images ●Segmentations of Cup and disc	http://medimrg.webs.ull.es/rim-one-dl-a-unified-retinal-image-database-for-assessing-glaucoma-using-deep-learning/
RIGA [28]	750			● Each image has six boundaries detection for OC and OD	https://deepblue.lib.umich.edu/data/concern/data_sets/3b591905z
DRIONS-DB [29]	110			● Contour OD by 36 points ● Software provided OD contours	http://www.ia.uned.es/~ejcarmona/DRIONS-DB.html
INSPIRE-AVR [30]	40			● Segmentation Optic Disc, Vessel and Arterio-venous ratio	https://medicine.uiowa.edu/eye/inspire-datasets
CHASE_DB1[31]	28			Vessel Segmentation	https://blogs.kingston.ac.uk/retinal/chasedb1/
ONHSD [32]	99			Optic Disc (OD) segmentation	http://www.aldiri.info/Image%20Datasets/ONHSD.aspx
DRIVE [33]	40			●Vessel Segmentation ●Mask FOV	http://www.isi.uu.nl/Research/Databases/DRIVE/
STARE [34][35]	402			● 13 diseases ● 81 locations optic disc, 10 locations veins and arteries, 20 blood vessels	http://cecas.clemson.edu/~ahoover/stare/
ARIA [36]	138		51	●Healthy and diseased ● Segmentation Vessel and OD ●Location of Fovea	http://www.damianjjfarnell.com/?page_id=276
DIARETDB0 [37]	130		20	●File signs of diabetic retinopathy ●software to annotate and inspect	https://www.it.lut.fi/project/imageret/diaretdb0/index.html
DIARETDB1 [38]	89		5	● Images point to signs diabetic ●software to annotate and inspect	https://www.it.lut.fi/project/imageret/diaretdb1/
MESSIDOR [39]	1200			Spreadsheet grade and risk of macular edema	https://www.adcis.net/en/third-party/messidor/
MESSIDOR-2 [40]	1748			Spreadsheet grades and referable diabetic macular edema grades	https://www.adcis.net/en/third-party/messidor/
ROC [41]	100			Diabetic retinopathy	http://webeye.ophth.uiowa.edu/ROC/
EyePACS/ DR Kaggle [42]	34000			5 levels for grading of the "Diabetic Retinopathy" (DR)	https://www.kaggle.com/c/diabetic-retinopathy-detection/overview

4. Performance Metrics

The most crucial applications in glaucoma diagnosis involve classification and segmentation. They require metrics for evaluating a method's efficiency. In general, the metrics for segmentation measure the degree of overlap or similarity between the segmentation result and the ground truth, while the metrics for classification measure the number of images classified correctly. Most metrics depend on True Positive (TP), False Negative (FN), True Negative (TN), and False Positive (FP). They represent the results of segmentation (in pixels) and classification (in the number of images). Both operations (segmentation and classification) can be seen as classifications since the segmentation (binary classification) divides pixels into classes. There are two deceptions in classification and segmentation contained within these terms. This work distinguishes between all metrics used for segmentation by putting x refers to pixel ($*_x$) such as sensitivity for segmentation (SEN_x) versus for classification (SEN). Table 3 shows the segmentation and classification metrics.

Table 3-Segmentation and classification metrics

Metrics	Abbreviation & Formula
Sensitivity/ Recall	$SEN_x = TP_x/(TP_x + FN_x)$
Specificity	$SPE_x = TN_x /(TN_x + FP_x)$
Accuracy	$ACC_x = (TP_x + TN_x)/ (TP_x + FN_x + TN_x + FP_x)$
Precision	$PRE_x = TP_x/ (TP_x + FP_x)$
False Positive Rate	$FPR_x = FP_x/(FP_x + TN_x)$
Dice/F- score	$DICE_x = 2 * TP_x/(2 * TP_x + FP_x + FN_x)$
Intersection-Over-Union / Jaccard	$IoU_x = TP_x/ (TP_x + FP_x + FN_x)$
Overlapping Error	$OER_x = 1 - [Area(Ground \cap result)/Area(Ground \cup result)]$
Relative Area Difference	$RAD_x = \big(Area(Ground) - Area(result)\big) /Area(result)$
Correlation Coefficient	$CC_x = coverance\ (x,y)/ S_x S_y$
Absolute CDR error	$ACDRE_x = \lvert CDR_{result} - CDR_{Ground\ Truth} \rvert$
Area Under the Curve	AUC_x= A curve that represents the nonlinear function between Sensitivity and (1− Specificity)
Average Boundary Distance	$AVRBD_x = \frac{1}{N}\sum_{\varphi=1}^{\varphi N} \sqrt{\left\lvert (D_G^{\varphi})^2 - (D_R^{\varphi})^2 \right\rvert}$,B_G, B_R boundaries ground truth and result. (D_G^{φ}) and (D_R^{φ}) distances from the points on (B_G) and (B_R) to the centroid of (B_G), in the direction of φ_N where N=4, $\varphi = 270^{\circ}, 180^{\circ}, 90^{\circ}$ and 0°

5. Enhancement Retinal Image

Most computer vision and image processing applications apply a preprocessing step, which improves the raw image and makes it more suitable for work, such as: image fusion, de-noise, de-blur, and de-haze applications ([43], [44]). Analyzing and diagnosing glaucoma based on fundus retinal images requires a preprocessing step because the low-resolution of the image with unclear details makes it difficult to diagnose a disease, particularly in automatic systems. The processes of glaucoma diagnosis are interrelated. Hence, the enhancement of the image influences the accuracy of the results of the segmentation step and so on [45]. Therefore, it is necessary to overcome the challenge of poor image resolution through image enhancement algorithms. Table 4 shows an overview of articles enhancing the retinal image.

Table 4-Overview of articles for enhancing the retinal image.

Author/s	Method	Dataset
Dai et al. 2016 [46]	●Normalized convolution, domain transform ●Image Fusion	●DRIVE (40) ●DIARETDB1

	●A fourth-order partial differential equation for noise removal to avoid the blocky effects and the relaxed median filter	(89) ●STARE (402)
Zhou et al. 2017 [45]	●Reducing the size of the image ●Enhancement luminosity by a gain matrix based on gamma correction for V channel ●Enhancement contrast for L channel by "Contrast Limited Adaptive Histogram Equalization" (CLAHE).	● MESSIDOR(1200) ● Private (961)
Palanisamy et al. 2018 [47]	●Enhancement luminosity by gamma correction based on "Cumulative Density Function" (CDF) for the V channel. ●Modified the histogram based on mean Structural Similarity Index SSIM ● Enhanced contrast based on CLAHE to the low-frequency components in "Discrete Wavelet Transform" (DWT)	Private (128)
You et al. 2019 [48]	Cycle-CBAM modified the CycleGAN by utilizing the "Convolutional Block Attention Module" (CBAM)	● EyePACS (88702) ● Private (2906)
Luo et al. 2020 [49]	●Created synthesized cataract-like images from a clear image by applying the mathematical haze model and refined image by CNN called CataractSimGAN ●De-hazing image by using CNN called CataractDehazeNet	private (800)
Aurangzeb et al. 2021 [50]	Modifying "Contrast Limited Adaptive Histogram Equalization" (CLAHE) by "Modified Particle Swarm Optimization" (MPSO) For Green channel	● DRIVE (40) ● STARE (40)
Wang et al. 2021 [51]	●Separated the image into three layers using Total-Variation ●The base for correcting the illumination, details for enhancing the contrast, and noise for smoothing the image	●DIARETDB0 (130) ●DIARETDB1 (89)

6. Localization Optic Disc/ Optic Nerve Head (ONH)

The optic disc (OD) is the key to identifying many diseases, so the localization of OD is an essential step for retinal fundus image analysis to reduce the time and increase the accuracy of the work [52]. In general, the OD is the bright circular region in the retinal fundus image [53]. The region of interest (ROI) is the area that contains the OD. The optic nerve head (ONH) is the other name for the OD. Some articles consider the ONH as the ROI. Table 5 shows an overview of some localization methods.

Table 5-Overview of articles for localization Optic Disc (OD)/ Optic Nerve Head (ONH).

Author/s	Preprocessing	Localization	Dataset
Alghamdi et al. 2016 [52]	Subtracted the average and divided by standard deviation	Cascade classifier with CNN	MESSIDOR (1200),STARE (402), DIARETDB1 (89), DRIVE (40), Four local (4050)
Wu et al. 2016 [53]	●Removing the cross of the vessels by morphology operations ●Computing the gradient direction of the OD without vessels	"Hybrid Directional Model" (HDM) by Incorporating two-directional models ● "Relaxed Bi-parabola Directional Model" (R-BPDM) ● "Disc Directional Model"	STARE (81), ARIA (120) MESSIDOR (1200), ROC (100) DIARETDB0 (130), DRIVE (40) DIARETDB1 (89), ONHSD (90) DRIONS (110)
Peiyuan et al. 2017 [54]	Subtracted the average and resized images	VGG CNN	STARE (400), ORIGA (650) MESSIDOR (1200)
Martinez-Perez et al. 2019 [55]	●For ONH "Reduced size of image, ●Created mask of the FOV by Otsu, increase the contrast ●Removed smaller objects such as blood vessels by using Gaussian filter	●Otsu: multi-level thresholding ●Combined channels based on binary operations ●Selected the object with large roundness	Private(1131) DRIVE (40) MESSIDOR (1200)

	●For OD center: Removed blood vessels using morphological operations ●Selected one channel from RGB image based on Shannon information	OD center: circular Hough transform	

7. Segmentation in Retinal Fundus Image

Accurate segmentation for regions of the retinal fundus image is necessary to solve the challenge of the accuracy of diagnosing diseases in automatic systems. The segmentation step is usually performed before the classification step because the classification step analyzes specific regions within the fundus image. As seen in Figure 1, the regions of the retinal fundus image that are considered important regions based on the classification method. The regions are the optic disc (OD), optic cup (OC), blood vessel, and Fovea. The optic disc and the optic cup are the main parts in fundus images that most of the methods need to be segmented. There are several articles for segmentation fundus images. They are categorized according to the article's objective.

7.1 Segmentation Blood Vessels

Blood vessels are a vital component in the fundus image. There are some purposes for segmenting blood vessels. The first purpose is to segment vessels and study their properties and the correlation of these properties with diagnosing diseases. The extracted properties are color, size, and shape. The second purpose is to segment the vessels and track their path and curvature for extracting some cues to determine the position of the OC and OD (bending in the border of the optic cup and entering the vessels into the optic disc from the top and bottom). The third purpose is to segment blood vessels for the purpose of removing them in a precise way**.** Table 6 shows an overview of a set of articles that aim to segment blood vessels.

Table 6-Overview of articles for blood vessels segmentation methods

Author/s	Preprocessing	Segmentation	Performance Metrics %				Dataset
			AUC,	ACC$_x$	SEN$_x$	SPE$_x$	
Hu et al. 2018 [56]		●Multi-scale CNN supported with a modified cross-entropy function ●Fully connected "Conditional Random Fields" (CRFs)	97.59	95.33	77.72	97.93	DRIVE (40)
			97.51	96.32	75.43	98.14	STARE (20)
Gu et al. 2019 [57]	Scaling image, HSV color space, Shifting randomly, Data augmentation	New "Context Extractor Network" (CE-Net)	97.79		83.09	95.45	DRIVE (40)
Jin et al. 2019 [58]	Reduced image size, Normalized ●Enhanced contrast by "Contrast Limited Adaptive Histogram Equalization" and gamma	"Deformable U-Net" (DUNet)	98.02	95.66			DRIVE (40)
			98.32	96.41			STARE (20)
			98.04	96.1			CHASE (28)
			98.31	96.51			HRF(45)
KHAN et al. 2021 [59]	●Getting Gray image by using Principal Component Analysis ●Smoothing by the median filter.	"Normalized Second-Order Derivative of anisotropic Gaussian Kernel" (NSDAGK)		95.2	78.5	96.7	DRIVE (40)
				95.1	78.8	96.6	STARE (20)
				95.21	96.82	78.75	CHASE (28)

7.2 Segmentation of the Optic Disc

This section presents a set of articles for the segmentation of the optic disc (OD), as shown in Table 7. For segmentation of the OD, the methods of localizing the OD (section 6) and segmenting blood vessels (section 7.1) can be used as preprocessing.

Table 7-Overview of articles for Optic Disc (OD) segmentation methods

Author/s	Preprocessing	Localization	Segmentation	Performance Metrics %					Dataset
				DICE	IoU_x	ACC_x	SEN_x	SPE_x	
Abdullah et al. 2016 [60]	●Normalizing G channel by subtracting smoothing version from morphology version ● Remove vessel by morphology operation	Circular Hough transform	Grow-cut	87.2	78.6	97.72	81.87	99.66	DRIVE (40)
				89.10	85.1	97.72	85.10	99.84	DIARETDB1 (89)
				90.50	83.2	95.79	83.13	99.71	CHASE_DB1 (28)
				91.02	85.1	95.45	85.08	99.66	DRIONS-DB (110)
				93.39	87.93	99.89	89.54	99.95	MESSIDOR (1200)
				87.63	80.1	97.93	80.15	99.91	Private: (19)
				91.97	86.1	99.67	88.57	99.92	ONHSD (99)
Zahoor et al. 2017 [61]	●Corrected illumination by Histogram Matching ●Normalizing Red channel by subtracting ● Remove vessel ●Improved the OD Circular boundary by morphology operation	●Estimated the center of OD ●Hough Transform	● Cropping ROI ● Polar transform ● Morphology operations ●Adaptive thresholding ●Ellipse fitting	90.39	84.4	99.18	88.91	99.73	MESSIDOR (1200)
				93.06	87.4	99.37	97.06	99.49	DIARETDB1 (89)
				93.78	88.6	99.86	93.84	99.94	DRIONS-DB (110)
				85	75.6	99.8	83.09	99.93	DRIVE (40)
				84.91	74.8	97.5	91.12	98.07	RIM-ONE (118)
				92.82	86.86	97.74	92.33	98.92	HRF (45)
				93.32	87.88	99.63	89.08	99.96	Private: (111)
Ramani et al. 2020 [62]	●Resized image ●Binarized image ●Eroded image ●Multiplied bitwise ●Smoothed by Gaussian filter	●Smoothed Green by opening ● CLAHE ●Binarized images ●Applied pixel density calculation and multilevel localization	●Cropped image ●Circular Hough ●Super Pixel segmentation	89.62	82.17	99.37	92.49	99.59	DRIONS-DB (110)
				88.43	80.05	99.31	95.82	99.43	DRISHTI (101)
				85.42	75.59	99.72	83.76	99.89	MESSIDOR (1200)
				81.38	71.00	99.38	90.35	99.52	DRIVE (40)
				85.98	77.11	99.20	91.26	99.43	CHASE_DB1 (28)
				85.43	75.47	99.31	80.35	99.84	INSPIRE-AVR (40)
				88.23	80.18	99.67	85.21	99.90	HRF (45)
				84.48	74.04	99.64	85.47	99.82	ONHSD (90)

7.3 Segmentation of the Optic Cup

The location of the optic cup (OC) is inside the optic disc. Figure 1 shows the structure of the fundus image and refers to the OC. In the fundus images, the segmentation of the OC is the most challenging task since the OC interferes with the OD and blood vessels are present, in addition to the distortions that are observed in this area due to the disease. This section presents a set of articles for the segmentation of the OC. Table 8 shows methods for segmenting OC.

Table 8-Overview of articles for Optic Cup (OC) segmentation methods

Author/s	Preprocessing	Segmentation	Performance Metrics %			Dataset
			DICE$_x$	ACC$_x$	AVRB	
Yang et al. 2018 [63]	●Enhanced Green by morphological operations ●Subtracted the smoothed version from the enhanced version ●Inpainting blood vessels	"Local Chan–Vese" (LCV)	79.55		12.32	private (94)
Pruthi et al. 2020 [64]		"Glowworm Swarm Optimization" (GSO) algorithm		98.61		RIM-ONE (159)
				100		DRIVE (40)
				98.75		STARE (81)
			94	99.87	23.8	DRIONS-DB (110)
				96.56		DIARETDB1 (89)
Prastyo et al. 2020 [65]	Cropped the rectangular region around the optic disc manually	Modified the architecture of U-Net	98.42			ORIGA (650)

7.4 Segmentation of the Optic Disc, Fovea, and Blood Vessel

This section presents several articles that aim to segment more than one part of the fundus images, such as the optic disc, fovea, and blood vessels. Table 9 shows the brief steps of the articles.

Table 9-Overview of articles for Optic Disc, Fovea, and blood vessel segmentation methods

Author/s	Preprocessing	Localization	Segmentation	Performance Metrics %					Dataset/ Work on
				IoU	ACC$_x$	SEN$_x$	SPE$_x$	PRE$_x$	
Rodrigues et al. 2017 [66]	Selected the best contrast channel	Bright region	Transforming into Haar 5th level wavelets and threshold		85				DRIVE (40)/ OD
	Selected Green channel		Vessels: multi-scale Frangi based on Hessian matrices		92.69				DRIVE (40)/ vessels
Kim et al. [67]	Selected the Green channel ●Removed noise (Gaussian) ●enhanced contract (CLAHE)		●Smoothing the Green channel by morphological operations ●Differencing the morphology version and enhanced version ●Applied Otsu method		95.35	75.17	97.24	73.40	DRIVE (40)/ vessels
		●Binarized the enhanced version ●Determined circle-shaped around OD	●Enhanced contract ●Removed the vessels of ROI ●Reconstructed the OD region by using Otsu		99.18	78.22	99.54	77.16	DRIVE (40)/ OD
					98.94	91.08	99.21		DRIONS-DB (110)/ OD
		Determining circle-shaped center vessels (ROI)	●Differencing the morphology version and flood-fill version ● Applied Otsu method		99.80	90.60	99.85	78.42	DRIVE (40)/ Fovea
Carmona et al. 2021[68]	●Reduced the size of the image, flipped		●Learned simultaneously " Intra-Structure Relational Knowledge" (intra-SRK),	84.2	99.79				ONHSD (99)/ OD
				87		90.7	99.9		MESSIDOR

	horizontally the image to the left side ●Normalized the image by using contrast stretching		and (inter-SRK) models ●Combined the intra-SRK and inter-SRK models to create an OD-fovea model ●Differential evolutionary			2	5		(1200)/ OD
						88.41	99		MESSIDOR (1200)/ Fovea

7.5 Segmentation Optic Disc and Optic Cup

There are two kinds of segmentation. The first kind is joint segmentation, where the result of segmentation contains the optic disc and the optic cup as one region. The second kind is disjoint segmentation, where the result of segmentation consists of two independent regions: the optic disc and the optic cup regions. Table 10 shows the articles of the joint segmentation and Table 11 shows the articles of the disjoint segmentation.

Table 10-Overview of articles for joint segmentation methods.

Author/s	**Preprocessing**	**Localization**	**Joint OD&OC Segmentation**	**OD/ OC**	**Performance Metrics %**						**Dataset**
					DICE$_x$	**IoU$_x$**	**ACC$_x$**	**SEN$_x$**	**SPE$_x$**	**PRE$_x$**	
Shankaranarayana et al. 2017 [69]	Resize image 256× 256		ResU-cGAN	OD	97.7	89.7					RIM-ONE (159)
				OC	94	76.8					
Tabassum et al. 2020 [70]	●Reduced the size ● Augmented the images		CNN called CDED-Net	OD	95.97	91.83	99.66	97.45	99.73		DRISHTI-GS (101)
				OC	92.4	86.32	99.71	95.67	99.81		
				OD		88.37					REFUGE (400)
				OC		81.11					
				OD	95.82	91.01	99.56	97.34	99.73		RIM-ONE (159)
				OC	86.22	75.32	99.61	95.17	99.81		
Liu et al. 2021[71]	Data augmentation	Extracted the ROI by CNN U-net and circular Hough	CNN called DDSC-Net	OD	97.8	95.7		97.84		97.78	DRISHTI-GS (101)
				OC	91.23	84.42		92.2		91.49	
				OD	96.01	92.39		98.14		94.12	REFUGE (120)
				OC	89.03	80.65		92.09		87.49	

Table 11-Overview of articles for disjoint segmentation methods

Author/s	**Preprocessing**	**Localization**	**Disjoint OD&OC Segmentation**	**OD OC**	**Performance Metrics %**					**Dataset**
					DICE$_x$	**IoU$_x$**	**ACC**	**SEN**	**PRE$_x$**	
Mittapalli and Kande 2016 [9]	Detected and removed blood vessels	"Principal component analysis" (PCA)	Active contour "spatially weighted fuzzy c means"	OD	97.5					Private (40) RIM-ONE (10) DIARETDB0 (9)
				OC	89					
Sevasto-polsky et al. 2017 [72]	● CLAHE ●Augmenting data		Modification of U-Net CNN	OD	94	89				DRIONS-DB (110)
					95	89				RIM-ONE-r3 (159)
	●Cropping OD		==	OC	82	69				

	•CLAHE •Augmenting data				85	75				DRISHTI-GS (50)
Nazir et al. 2021 [73]	•Augmented data •Created a polygon for OD and OC using "VGG Image Annotator" (VIA)	•Created features map using DenseNet-77 •Identified ROI using "Region Proposal Network"	Custom Mask-R-CNN •Improved location of OD and OC •Created Mask for OD and OC	OD	95.3	98.1	97.9	96.9	95.9	ORIGA (650)
				OC	98.7	96.3	95.1	95.7	97.1	

8. Glaucomatous Classification

Retinal funds Image classification is the backbone of this study because correctly classifying the images leads to an accurate diagnosis of glaucoma. There are multiple methods for classifying images (for glaucoma diagnosis). This study categorizes the classification methods according to the type of features used in the classification. The following subsections describe the classification methods: medical-based techniques; intensity-based techniques; deep-based techniques; and hybrid-based techniques.

8.1 Medical-Based Techniques

This section presents the first category of the Retinal Fund's image classification. The first category is the method that depends on the structural characteristics. The characteristics are used clinically in the diagnosis of glaucoma diseases, such as the Cup-to-Disc Ratio (CDR). The study will call this category a medicinal-based technique. Table 12 shows the articles in the first category.

Table 12-Overview of articles for glaucoma diagnosis (Medical-Based Techniques)

Author/s	Preprocessing	Localization	Segmentation	Features Extraction for Classification	Measure	Value%	Dataset
Ayub et al. 2016 [74]	Removing vessels, Sharping and Equalizing image	•Intensity weighted centroid then cropped the ROI	•K-mean clustering for L channel •Canny and ellipse fitting	• CDR	ACC	92	Private (100)
					SEN	93	
					SPE	88	
Zilly et al. 2017 [75]	After localization •L∗ a ∗b •Subtracted by mean •Division by standard deviation	•Circular Hough for Green • Cropped ROI	•Reduce computation •CNN with Gentle AdaBoost •Graph cut algorithm •Convex hull	• CDR	SEN	92.3	RIM-ONE (159)
					SPE	95.6	
					ACC	94.1	
Arnay et al. 2017 [10]	Segmented vessels by thresholding & thinning		"Ant Colony Optimization" (ACO)	• CDR	AUC	79.57	RIM-ONE (159)
Huazhu et al. 2018 [6]	Multiple sizes with polar transformation version images		• M-Net CNN with 4 mechanism • threshold, ellipse fitting for segmenting jointly OD and OC	• CDR • RDAR	AUC	85.08	ORIGA (650)
					AUC	89.97	Private (1676)
Nawaldgi et al. 2018 [12]			Thresholding and morphology operations •OD from Red •OC from Green	• CDR • ISNT rule	ACC	99	DRISHTI-GS1 (101)

Mohamed et al. 2019 [76]	● Selection channel ● Noise removal by Anisotropic Diffusion ● Corrected the illumination		● Superpixels based on "Simple Linear Iterative Clustering" ●Extraction features by "Statistical Pixel-Level" ●Support Vector Machine for OD&OC	● CDR ● CDAR	AUC	91	RIM-ONE (166)
					SEN	92.30	
					SPE	97.60	
					AUC	98.63	
Riaz et al. 2020 [77]	● Estimated the size of OD ●Illumination correction ● Data augmentation	Template matching	Fuzzy broad learning system ●Level-1(OD: Red) ●Level-2(OC: Green)	● CDR	AUC	90.6	RIM-ONE-r3 (159)
					AUC	923	Private (566)
					AUC	97.21	REFUGE (1200)
					AUC	88.7	DRISHTI-GS (101)
Imtiaz et al.2021 [78]	● Reducing the size of the images ● Augmenting data by contrast variations and rotation		● Encoder-decoder based on Semantic Segmentation fine tuning VGG 16 CNN ● Removing noise ●Ellipse fitting	● CDR	SEN	96.74	RIM-ONE-r3 (169)
					SPE	99.1	
					ACC	99.03	
					DICE	85.94	

8.2 Intensity-based Techniques

The second category is the method that depends on pixels' features to classify the image. Statistical features are an example of them. Intensity-based techniques fall into the second category. The set of articles showing intensity features is in Table 13.

Table 13-Overview of articles for glaucoma diagnosis (Intensity-based Techniques)

Author/s	Preprocessing	Localization	Segmentation	Features Extraction	Norm./ Selection	Classification	Measure	Value%	C.	Dataset
Maheshwari et al. 2016 [14]	Extracting R, G, B, and gray			●**Transforming into** "Empirical Wavelet Transform" (EWT) ●Extracting 3 Correntropy features for each channel	T-test/ z-score	" Least Squares Support Vector Machine " (LS-SVM)	ACC	98.33	3-f.	Private (60)
							ACC	96.67	10-f	
							ACC	81.32	3-f.	RIM-ONE (505)
							ACC	80.66	10-f	
Singh et al. 2016 [79]		●Kaiser window for getting high intensity from Green ●cropped circular ROI	●Segmenting OD by bit plane from R channel ●Removing vessels by the in-painting method	●**Transforming into** first level Discrete wavelet (DWT) ●Extracting mean and energy using Haar, db3, Symlet3 and Bi-orthogonal filters	Genetic, Evolutionary Attribute	Random forest	ACC	94.75		Private (63)
						Naïve Byes	ACC	89.48		
						ANN	ACC	94.75		
					z-score/ "Principal Component Analysis"	SVM	ACC	94.75		
						K-NN	ACC	94.75		
Kavya et al. 2017 [80]	enhance R by "Adaptive Histogram Equalization"		Hough Transformation for OD	● "Gray Level Co-occurrence Matrix" ● "Gaussian Markov Random Field" (MRF)		"Support vector machine" (SVM)	ACC	86		DRISHTI-GS(101), Private: (30)
Maheshwari et al.	●Resized images			●**Transforming into** "Variational	Z-score/ Relief	"least squares	ACC	94.79	10-f.	Private(488)

2017 [4]	• Enhanced by CLAHE			Mode Decomposition" (2D-VMD) • Extracting entropies and fractal dimensions		support vector machine" (LS-SVM)	SEN	93.62		
							SPE	95.88		
							ACC	95.16	3-f.	
							ACC	81.63	10-f.	RIM-ONE (505)
							ACC	81.22	3-f.	
Arwa A. Gasm Elseid and Alnazier O. Hamza 2018 [81]	•Resized the image •Smoothed the Red channel •Removed vessel •Enhanced the contract		OD thresholding smoothed and constructed a circle from the Red channel. OC used OD mask for thresholding and smoothed	13 shape features from OD and OC	T-test	Ensemble RUSBOOSTED tree classifier with SMOTE method	SEN	85.1	f.10	RIM-ONE (169)
							SPE	93.6		
							ACC	91.3		
							AUC	92		
Abdel-Hamid 2020 [82]	•Cropped the image •corrected illumination Red by subtracting mean •Smoothing and CLAHE	thresholding Red detected manually the radius, center, and rectangular for OD	Cropped rectangular boundary for OD for Green and Blue channels.	**•Transforming into** Daubechies4 wavelet • Textural features Extracted "Gray-Level Co-occurrence Matrices" (GLCM) features • Statistical features seven features	Relief algorithm and Information Gain	KNN classifier	AUC	92.2	5 f.	GlaucomaDB (66)
							ACC	89.4		
							SPE	90.9		
							SEN	87.9		
							AUC	94.7	5 f.	HRF (30)
							ACC	96.7		
							SPE	100		
							SEN	93.3		
Padma et al. 2021 [83]	•Removing noise by Median filter •Removing vessels by morphology operations	directional match filters cropped ROI	"Local Region Recursive Segmentation" (LRRS)	**•Transforming into** Empirical Wavelet Transform" (EWT) •Extracting: local binary pattern, local vector pattern, and correntropy features	Z-score / T-test	Random forest	SEN	89.29		RIM-ONE-r2 (455)
							ACC	89.71		
Shanthamalar J. Jeslin 2021 [5]		Localized OD by pixel density calculation	Cropped ONH	**•Converting into** 9 color model and gray •Extracting: Statistical, "Gray Level Concurrence Matrix" and Histogram features	Fisher filtering runs filtering and relief filtering	"Random Tree" (RT) classifier	ACC	96.83		DRISHTI-GS1 (101)
							SEN	97.26		RIM-ONE-r1 (169)

* (Norm.) refers to normalization, (C.) refers to cross-validation and (f.) refers to k-fold.

8.3 Deep-Based Techniques

The third category is the methods that depend on the deep features extracted through the Convolution Neural Network (CNN) to classify images. Table 14 shows a set of methods for deep-based techniques.

Table 14-Overview of articles for deep-based techniques to detect glaucoma

Author/s	Preprocessing	Localization	Segmentation	Features Extraction/ Classification	Measure	Value%	C.	Dataset
Abbas 2017 [18]		High intensity of Green channel	Croup the ROI	●Pre-trained CNN ●Optimized by the fine-tuning deep-belief network (DBN)	SEN	84.5	10-f.	● DRIONS-DB(110) ● HRF (30) ●sjchoi86-HRF(401) ●private (659)
					SPE	98.01		
					ACC	99		
					PRE	84		
Li et al. 2018 [84]	●Normalize ●Reduced size ●Subtracted mean ● Augmentation			Glaucomatous Optic Neuropathy" (GON) consisted of 11 Inception-v3 CNN	AUC	98.6		Private (48116)
					SEN	95.6		
					SPE	92		
					AUC	98.6		
Fu et al. 2018 [85]	● The stream of polar transformation work as data augmentation		CNN like the U-Net	●DENet with several streams based on fine-tuned for ResNet-50 Global Image, ONH, ONH polar, optic disc ●Ensemble Networks	AUC	91.83		private: SCES(1676)
					SEN	84.78		
					SPE	83.80		
					AUC	81.73		private: SINDI(5783)
					SEN	78.76		
					SPE	71.15		
Christopher et al. 2018 [86]	● Augmentation ●Reducing the size of the image	●Manually ●Learning model	Cropped the square around OD manually	Native ResNet50	AUC	89	10-f.	Private (7411)
				Transfer learning ResNet50	AUC	91		
Raghavendra et al. 2018 [87]	Reducing size image to 64*64 pixels			New CNN with 18 layers	ACC	98.13	5-f.	Private (1426)
					SEN	98.		
					SPE	98.3		
					PRE	98.79		
Ahn et al. 2018 [16]	●Cropped the optic nerve ●Data augmentation			Transfer learning of GoogleNet Inception	ACC	93		HARVARD (1542)
					AUC	84.5		
				New Convolutional Neural Network	ACC	87.9		
					AUC	94		
Diaz et al. 2019 [15]	●Subtracted the average ●Resized images ●data augmentation	Fine-tune VGG + thresholding	Croup the ROI	Fine-tuned Xception	AUC	96.05	10-f.	●ACRIMA (705) ●DRISHTI-GS1(101) ●sjchoi86-HRF (401) ● HRF (45) ●RIM-ONE (455)
					ACC	89.77		
					SPE	85.8		
					SEN	93.46		
					DICE	90.51		
Li et al. 2019 [22]	Resized images to 224 × 224	"Pathological Area Localization Subnet"		"Attention-based CNN for Glaucoma detection" AG-CNN: three stages "Attention Prediction	ACC	95.3		LAG(5824)
					SEN	95.4		
					SPE	95.2		
					AUC	97.5		

		(PALS)		Subnet" , "Pathological Area Localization Subnet" and "Glaucoma classification subnet"	ACC	85.2		RIM-ONE-r1 (169)
					SEN	84.8		
					SPE	85.5		
					AUC	91.6		
Serte et al. 2020 [88]	Data augmentation	Graph saliency region detection	Threshold cropped around OD	Three parallel fine-tuned CNNs AlexNet8 ResNet-50 and -152 ● Sum of the Maximal Probabilities" (SMP)	AUC	94		HARVARD (1542)
					ACC	88		
					SEN	86		
					SPE	90		
Hemelings 2020 et al. [89]	● Cropped square ●Resize image ● Gaussian ●Augmentation			●Transfer learning ResNet-50/ new layers ●Active learning and Saliency maps	AUC	99.5		Private (4935)
					SEN	98.0		
					SPE	91		
Joshi et al. 2020 [90]	●Data augmentation		Drew a bounding box manually	Transfer Learning of YOLO-v3	ACC.	93.7	5-f.	●DRISHTI-GS (101) ● REFUGE (400) ● private (256)
					SEN	89.1		
					SPE	95.85		
Alghamdi et al. 2021 [91]	Data augmentation			"Semi-supervised Convolutional Neural Network model with Autoencoder"	ACC	93.8		● RIM-ONE-r2 (455) ● RIGA (750)
					SEN	98.9		
					SPE	90.5		
					AUC	95		
Bao et al. 2021 [92]	Resized of images			"Self-Adaptive Transfer Learning" (SATL) integrated the VGG and "Variational Auto-Encoder" (VAE)	ACC	74		LAG (4854) private (1881) REFUGE-2 (400)
					SEN	71.38		
					PRE	59.55		
					DICE	57.1		

*(C.) refers to cross-validation and (f.) refers to k-fold

8.4 Hybrid-Based Techniques

The fourth category is the methods that depend on more than one type of feature. They combine more than one type of category. This type we will call the hybrid-based technique. The study presents two groups for this category: hybrid-based (Intensity + Medical) techniques in Table 15 and hybrid-based (Intensity + Deep) techniques in Table 16.

Table 15-Overview of articles for hybrid-based (Intensity + Medical) techniques to detect glaucoma

Author/s	Preprocessing	Segmentation	Features Extraction	Classification	Measure	Value%	C.	Dataset
Chakravarty et al. 2016 [8]	illumination correction	Template match by Hough to Crop square ROI	"Texture of Projection" (ToP) and "Bag of Words" (BoW)	"Support Vector Machine" (SVM)	ACC	76.77	5-f.	DRISHTI-GS1 (101)
					AUC	78		
		OD and OC by the estimated depth and "Markov Random Field"	●vertical CDR and rim to disc area ratio, major axis length of OD, and the ratio of horizontal to vertical CDR		ACC	73.28	5-f.	Private (1103)
					AUC	79		
Khalil et al. 2017 [11]	●Increased the resolution by the bilinear interpolation method	OD (R channel) OC (B channel) ●thresholding ● Opening ●Convex hull	Hybrid Structural Feature-set ● CDR ● Rim to Disc Ratio (RDR) ●"Hausdorff's Fractal Dimension" (HFD)	"Support Vector Machine" (SVM)	SPE	88	10-f.	GlaucomaDB (100)
					SEN	77		
					ACC	83		
		●Cropping the region of OD	Hybrid Texture Feature-set ● OD(GLCM, 2D Discrete	==	SPE	92	==	==

	●Scaled image ●Increased the contrast of the image ● Cropped ROI	● Segmenting vessels in the rim by 2D Gabor, multilayered thresholding	Wavelet Transform", Grey-level run length, Fractal, brightness, Super-pixels, mean and standard deviation ●Rim vessels (Area, Mean, Kurtosis, Standard deviation, Variance Skew)		SEN	96		
					ACC	94		
Pathan et al. 2021 [2]	Removed the blood vessels from the Green channel	OD: Prewitt filter, applied the circle finder operation OD: decision tree OC: k-mean	● Medical features (CDR, RAR, and ISNT rule), ●Color features (entropy, mean, skewness, energy, standard deviation, and variance) ●Texture features "Grey Level Co-occurrence Matrix"	"Support Vector Machine" (SVM)	SPE	91.21		private (300)
					SEN	93.47		
					ACC	90		
					SPE	92.68	10 f.	DRISHTI-GS1 (101)
					SEN	100		
					ACC	95		

*(C.) refers to cross-validation and (f.) refers to k-fold, ("==") refers to the same procedures or materials (as above).

Table 16-Overview of articles for hybrid-based (Intensity + Deep) techniques to detect glaucoma

Authors	Preprocessing	Features Extraction	selection	Classification	Measure	Value%	C.	Dataset
Claro et al. 2019 [19]	Used five channels RGB and HS	●Morphology : Area, Perimeter, Convex Area, Diameter, and Extension ●Texture: LBP , GLCM, HOG, Tamura and GLRLM ● Deep features: using CNNs (CaffeNet, Vgg-f, Vgg-m, Vgg-s, VGG-19, AlexNet and Vgg-16)	gain ratio	Random forest (RF)	ACC	93.35	10-f	RIM-ONE-r1 (158) RIM-ONE-r2 (455) RIM-ONE-r3 (159) DRISHTI-GS1 (101)
					AUC	98		
					ACC	93.61	10-f	HRF (30) JSIEC (67) ACRIMA (705)
					AUC	97.5		
Chaudhary et al. 2021[93]	●Extracted Green channel ●Enhanced contrast by CLAHE	"Two Dimensional Fourier-Bessel Series Expansion based Empirical Wavelet Transform" to obtain sub-images ●Extracted features by utilizing "Gray Level Co-occurrence Matrix" (GLCM), chip histogram, and moment invariance	min-max/ "Principal Component Analysis" (PCA) / T-Test	SVM	ACC	90		RIM-ONE-r2 (455)
				random forest (RF)	ACC	95.51		RIM-ONE-r1 (169) RIM-ONE-r2 (455)
				Random forest (RF)	ACC	98.21		RIM-ONE-r1 (169)
	●Reduced size of Green channel ●Enhanced by CLAHE ●Augmented	"Two Dimensional Fourier-Bessel Series Expansion based Empirical Wavelet Transform" to obtain sub-images ●Extracted deep features by transfer learning of ResNet-50		Soft-max classifier	ACC	91		RIM-ONE-r1 (169) RIM-ONE-r2 (455) RIM-ONE-r3 (159) ORIGA (650) DRISHTI-GS1 (101)
					SPE	83		
					SEN	94		
					AUC	96		

*(C.) refers to cross-validation and (f.) refers to k-fold

9. Discussion and Analysis

● Dataset

The retinal fundus image has many datasets. Depending on the ground truth, each dataset can be used to solve a specific problem. Figure 3 shows the datasets that were used in this review.

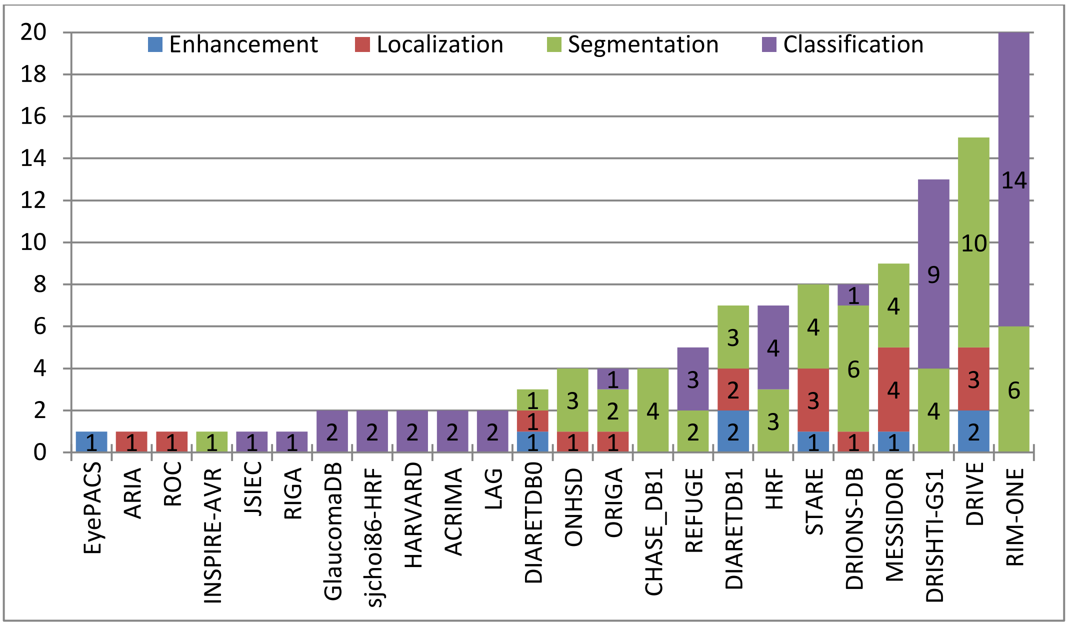

Figure 3-Categories of datasets used based on the presented articles.

●**Enhancement:** The enhancement image step is part of the preprocessing step. It includes correcting contrast/luminosity and de-noising. Several techniques such as CLAHE, gamma correlation, bilinear interpolation, subtracting mean, and CNN are utilized for adjusting contrast and luminosity, but CLAHE is the most widely used. De-noising can be done by using Gaussian, median, and anisotropic filters. The Gaussian filter is the most commonly used.

●**Localization:** The localization step of an optic disc (OD) is different from the OD segmentation step, but in many methods, the two steps overlap because the segmentation step initially needs to be localized. The localization step involves some tasks. The first task is to select a suitable channel, either using the Shannon information or the red channel, because it is the most common choice. The second task determines the work area, which is ONH or called ROI. The third task determines the center of the OD and sometimes its radius to be ready for segmenting. Notably, the Optic Cup does not need a localization step because the location of the OC is inside the OD and is usually identified by using the green channel.

●**Segmentation:** Segmentation is considered the most significant challenge in diagnosing glaucoma, especially when using classification methods based on medical features, because it requires very high precision segmentation. The purpose of segmentation is to extract OD and OC. Cup segmentation is the most difficult challenge in the diagnosis of glaucoma due to the overlap of the Cup with the Disc, the presence of blood vessels, and changes associated with glaucoma.

●**Classification**

▪ **Medical-based technique**: This type is the most important kind of classification because it uses the medical indicators for diagnosing glaucoma, such as the CDR and ISTR rules.

▪ **Intensity-based technique**: This type of classification has proven its worth, especially since it does not require precise segmentation. It extracts the features of the parts of the raw image or the converted version of the image (wavelet widely used) and afterwards classifies the features by one of the machine learning techniques (SVM widely used).

▪ **Deep-based technique:** The CNN net contains two stages: feature extraction (convolution layer and pooling layer) and a fully connected layer (classification). Practically, there are several kinds of CNN nets. First, the new CNN net (newly implemented) is built and trained from scratch. Second, the transfer learning net uses the pre-trained net and keeps the architecture and weights of the old net but makes a change in the fully connected layer (as retraining the weights and reducing the number of outputs). Third, the fine-tuning net uses the pre-trained net and retrains the weights (for any part of the net) or modifies any layer or parameter for the pre-trained net. Some methods use more than one kind (hybrid, transfer learning, and fine-tuning). However, in recent years, more methods that rely on CNN have achieved highly accurate results.

▪ **Hybrid-based techniques**: This type is comprehensive and extracts various features.
The hybrid-based (Intensity + Deep) technique archives good results.

10. Articles Gap

●Datasets

Methods using private datasets have a drawback because it is difficult to compare results with other methods and it is impossible to determine if the results are accurate. Some methods use inappropriate datasets with the target of the pepper consequence that the authors create private ground truth.

●Enhancement:

The enhancement must be precise because some methods generate blocky effects.

●Localization

Localizing the OD using only the principle that the OD is the bright circular region in the retinal fundus image is not accurate because the retinal fundus images contain a lot of bright areas. Some methods are not fully automatic, such as specifying the disc area and radius manually.

●Segmentation: Generally, if OD and OC are segmented by the same method, the segmentation results for OC will not be as pleasing. Most methods ignore the relationship between the parts of the retina.

●Classification

▪ **Medical-based technique:** It depends very heavily on the accuracy of separating the cup, disc, and the rest of the retina. However, there are several parameters associated with the features used in this type of classification. Most methods used one or two parameters and ignored the rest.

▪ **Intensity-based technique:** This type of work consumes a lot of time and effort. There are many extracted features, but the classification stage does not use all of them.

▪ **Deep-based technique:** It needs large datasets. Unfortunately, these are not available for glaucoma patients, as they consume a lot of time during training.

▪ **Hybrid-based techniques:** According to the best of our knowledge, no method combines the three kinds of features.

11. Conclusion and Guideline for Diagnosing Glaucoma

Analyzing the retina requires several major steps. The steps involve analyzing the retina based on the objective of the research and the techniques used by the researcher. The research goals are enhancement, localization, segmentation (several kinds), or classification. Classification usually has more steps than other applications. However, enhancement, localization, and segmentation are often implicit steps to achieve the goal of classification.
In glaucoma diagnosis, feature extraction and classification are indispensable steps, while the rest are used optionally depending on the methodology used in the algorithm. Figure 4 shows a summary of the main steps and useful notes required for glaucoma diagnosis.

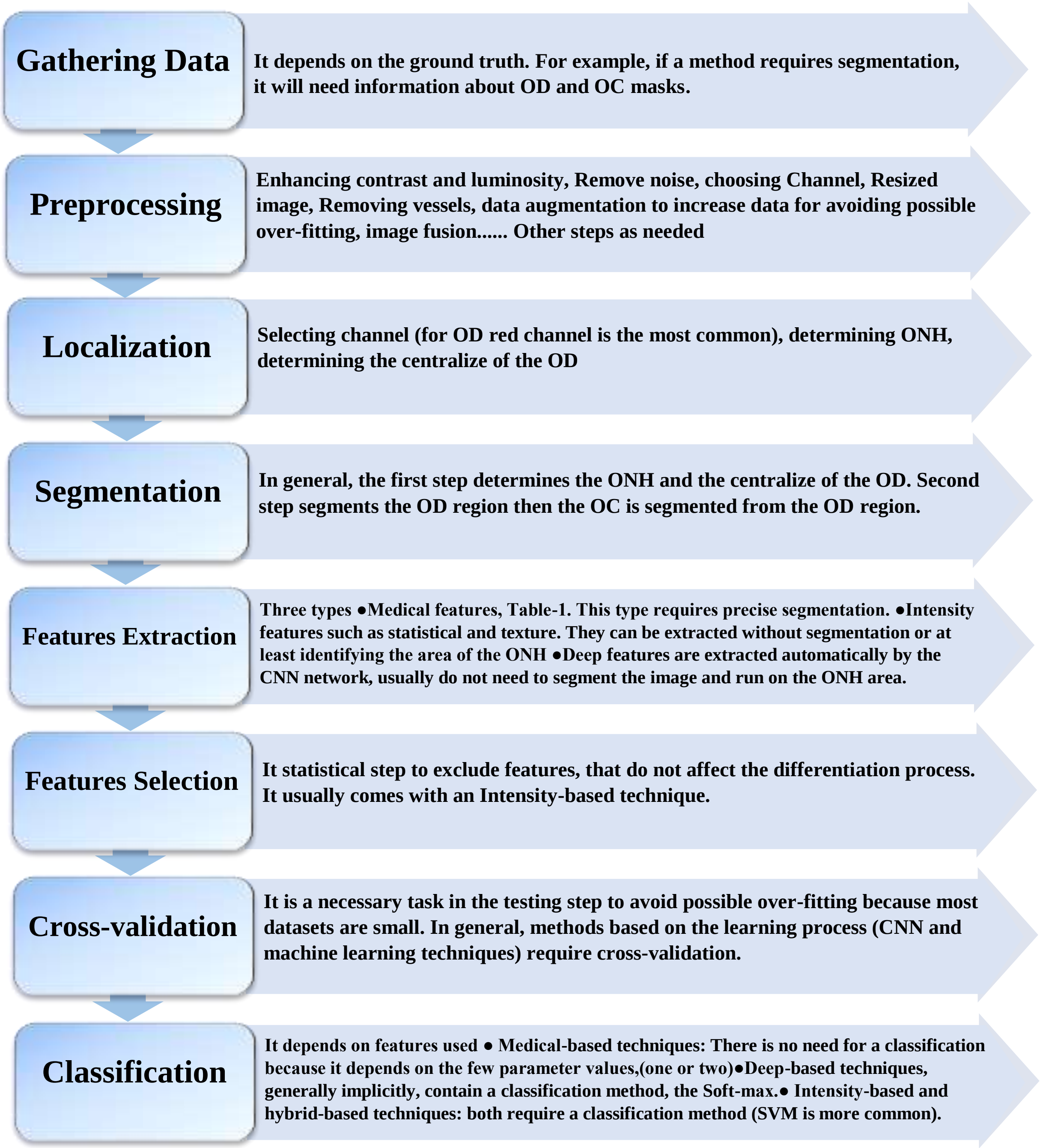

Figure 4-Guideline /Steps for diagnosing Glaucoma

12. References

[1] S. Sreng, N. Maneerat, K. Hamamoto, and K. Y. Win, “Deep learning for optic disc segmentation and glaucoma diagnosis on retinal images,” *Appl. Sci.*, vol. 10, no. 14, p. 4916, 2020.

[2] S. Pathan, P. Kumar, R. M. Pai, and S. V Bhandary, “Automated segmentation and classifcation of retinal features for glaucoma diagnosis,” *Biomed. Signal Process. Control*, vol. 63, p. 102244, 2021.

[3] R. Hemelings *et al.*, “Accurate prediction of glaucoma from colour fundus images with a convolutional neural network that relies on active and transfer learning,” *Acta Ophthalmol.*, vol. 98, no. 1, pp. e94–e100, 2020.

[4] S. Maheshwari, R. B. Pachori, V. Kanhangad, S. V Bhandary, and U. R. Acharya, “Iterative variational mode decomposition based automated detection of glaucoma using fundus images,” *Comput. Biol. Med.*, vol. 88, pp. 142–149, 2017.

[5] J. J. Shanthamalar and R. G. Ramani, "A Novel approach for Glaucoma Disease Identification through Optic Nerve Head Feature Extraction and Random Tree Classification," *Int. J. Comput. Digit. Syst.*, vol. 10, 2021.

[6] H. Fu, J. Cheng, Y. Xu, D. W. K. Wong, J. Liu, and X. Cao, "Joint optic disc and cup segmentation based on multi-label deep network and polar transformation," *IEEE Trans. Med. Imaging*, vol. 37, no. 7, pp. 1597–1605, 2018.

[7] B. Prabhakar, R. K. Singh, and K. S. Yadav, "Artificial intelligence (AI) impacting diagnosis of glaucoma and understanding the regulatory aspects of AI-based software as medical device," *Comput. Med. Imaging Graph.*, p. 101818, 2020.

[8] A. Chakravarty and J. Sivaswamy, "Glaucoma classification with a fusion of segmentation and image-based features," in *2016 IEEE 13th international symposium on biomedical imaging (ISBI)*, 2016, pp. 689–692.

[9] P. S. Mittapalli and G. B. Kande, "Segmentation of optic disk and optic cup from digital fundus images for the assessment of glaucoma," *Biomed. Signal Process. Control*, vol. 24, pp. 34–46, 2016.

[10] R. Arnay, F. Fumero, and J. Sigut, "Ant colony optimization-based method for optic cup segmentation in retinal images," *Appl. Soft Comput.*, vol. 52, pp. 409–417, 2017.

[11] T. Khalil, M. U. Akram, S. Khalid, and A. Jameel, "Improved automated detection of glaucoma from fundus image using hybrid structural and textural features," *IET Image Process.*, vol. 11, no. 9, pp. 693–700, 2017.

[12] S. Nawaldgi, Y. S. Lalitha, and M. Reddy, "A novel adaptive threshold and ISNT rule based automatic glaucoma detection from color fundus images," in *Data Engineering and Intelligent Computing*, Springer, 2018, pp. 139–147.

[13] R. Bock, J. Meier, L. G. Nyúl, J. Hornegger, and G. Michelson, "Glaucoma risk index: automated glaucoma detection from color fundus images," *Med. Image Anal.*, vol. 14, no. 3, pp. 471–481, 2010.

[14] S. Maheshwari, R. B. Pachori, and U. R. Acharya, "Automated diagnosis of glaucoma using empirical wavelet transform and correntropy features extracted from fundus images," *IEEE J. Biomed. Heal. informatics*, vol. 21, no. 3, pp. 803–813, 2016.

[15] A. Diaz-Pinto, S. Morales, V. Naranjo, T. Köhler, J. M. Mossi, and A. Navea, "CNNs for automatic glaucoma assessment using fundus images: an extensive validation," *Biomed. Eng. Online*, vol. 18, no. 1, pp. 1–19, 2019.

[16] J. M. Ahn, S. Kim, K.-S. Ahn, S.-H. Cho, K. B. Lee, and U. S. Kim, "A deep learning model for the detection of both advanced and early glaucoma using fundus photography," *PLoS One*, vol. 13, no. 11, p. e0207982, 2018.

[17] Z. Zhang *et al.*, "Origa-light: An online retinal fundus image database for glaucoma analysis and research," in *2010 Annual International Conference of the IEEE Engineering in Medicine and Biology*, 2010, pp. 3065–3068.

[18] Q. Abbas, "Glaucoma-deep: detection of glaucoma eye disease on retinal fundus images using deep learning," *Int J Adv Comput Sci Appl*, vol. 8, no. 6, pp. 41–45, 2017.

[19] M. Claro *et al.*, "An hybrid feature space from texture information and transfer learning for glaucoma classification," *J. Vis. Commun. Image Represent.*, vol. 64, p. 102597, 2019.

[20] M. U. Akram, A. Tariq, S. Khalid, M. Y. Javed, S. Abbas, and U. U. Yasin, "Glaucoma detection using novel optic disc localization, hybrid feature set and classification techniques," *Australas. Phys. Eng. Sci. Med.*, vol. 38, no. 4, pp. 643–655, 2015.

[21] J. I. Orlando *et al.*, "Refuge challenge: A unified framework for evaluating automated methods for glaucoma assessment from fundus photographs," *Med. Image Anal.*, vol. 59, p. 101570, 2020.

[22] L. Li, M. Xu, X. Wang, L. Jiang, and H. Liu, "Attention based glaucoma detection: A large-scale database and cnn model," in *Proceedings of the IEEE/CVF Conference on Computer Vision and Pattern Recognition*, 2019, pp. 10571–10580.

[23] J. Sivaswamy, S. R. Krishnadas, G. D. Joshi, M. Jain, and A. U. S. Tabish, "Drishti-gs: Retinal image dataset for optic nerve head (onh) segmentation," in *2014 IEEE 11th international symposium on biomedical imaging (ISBI)*, 2014, pp. 53–56.

[24] A. Budai, R. Bock, A. Maier, J. Hornegger, and G. Michelson, "Robust vessel segmentation in fundus images," *Int. J. Biomed. Imaging*, vol. 2013, 2013.

[25] F. Fumero, S. Alayón, J. L. Sanchez, J. Sigut, and M. Gonzalez-Hernandez, "RIM-ONE: An open retinal image database for optic nerve evaluation," in *2011 24th international symposium on computer-based medical systems (CBMS)*, 2011, pp. 1–6.
[26] F. Fumero, J. Sigut, S. Alayón, and M. González-Hernández, "Interactive tool and database for optic disc and cup segmentation of stereo and monocular retinal fundus images," *23rd International Conference in Central Europe on Computer Graphics, Visualization and Computer Vision, Czech Republic,* vol : short papers proceedings, 2015
[27] F. J. F. Batista, T. Diaz-Aleman, J. Sigut, S. Alayon, R. Arnay, and D. Angel-Pereira, "RIM-ONE DL: A Unified Retinal Image Database for Assessing Glaucoma Using Deep Learning," *Image Anal. Stereol.*, vol. 39, no. 3, pp. 161–167, 2020.
[28] A. Almazroa *et al.*, "Retinal fundus images for glaucoma analysis: the RIGA dataset," in *Medical Imaging 2018: Imaging Informatics for Healthcare, Research, and Applications*, 2018, vol. 10579, pp. 55–62.
[29] E. J. Carmona, M. Rincón, J. García-Feijoó, and J. M. Martínez-de-la-Casa, "Identification of the optic nerve head with genetic algorithms," *Artif. Intell. Med.*, vol. 43, no. 3, pp. 243–259, 2008.
[30] M. Niemeijer *et al.*, "Automated measurement of the arteriolar-to-venular width ratio in digital color fundus photographs," *IEEE Trans. Med. Imaging*, vol. 30, no. 11, pp. 1941–1950, 2011.
[31] M. M. Fraz, A. R. Rudnicka, C. G. Owen, and S. A. Barman, "Delineation of blood vessels in pediatric retinal images using decision trees-based ensemble classification," *Int. J. Comput. Assist. Radiol. Surg.*, vol. 9, no. 5, pp. 795–811, 2014.
[32] J. Lowell *et al.*, "Optic nerve head segmentation," *IEEE Trans. Med. Imaging*, vol. 23, no. 2, pp. 256–264, 2004.
[33] J. Staal, M. D. Abràmoff, M. Niemeijer, M. A. Viergever, and B. Van Ginneken, "Ridge-based vessel segmentation in color images of the retina," *IEEE Trans. Med. Imaging*, vol. 23, no. 4, pp. 501–509, 2004.
[34] A. Hoover and M. Goldbaum, "Locating the optic nerve in a retinal image using the fuzzy convergence of the blood vessels," *IEEE Trans. Med. Imaging*, vol. 22, no. 8, pp. 951–958, 2003.
[35] A. D. Hoover, V. Kouznetsova, and M. Goldbaum, "Locating blood vessels in retinal images by piecewise threshold probing of a matched filter response," *IEEE Trans. Med. Imaging*, vol. 19, no. 3, pp. 203–210, 2000.
[36] D. J. J. Farnell *et al.*, "Enhancement of blood vessels in digital fundus photographs via the application of multiscale line operators," *J. Franklin Inst.*, vol. 345, no. 7, pp. 748–765, 2008.
[37] T. Kauppi *et al.*, "DIARETDB0: Evaluation database and methodology for diabetic retinopathy algorithms," *Mach. Vis. Pattern Recognit. Res. Group, Lappeenranta Univ. Technol. Finl.*, vol. 73, pp. 1–17, 2006.
[38] R. Kälviäinen and H. Uusitalo, "DIARETDB1 diabetic retinopathy database and evaluation protocol," in *Medical Image Understanding and Analysis*, 2007, vol. 2007, p. 61.
[39] E. Decencière *et al.*, "Feedback on a publicly distributed image database: the Messidor database," *Image Anal. Stereol.*, vol. 33, no. 3, pp. 231–234, 2014.
[40] J. Krause *et al.*, "Grader variability and the importance of reference standards for evaluating machine learning models for diabetic retinopathy," *Ophthalmology*, vol. 125, no. 8, pp. 1264–1272, 2018.
[41] M. Niemeijer *et al.*, "Retinopathy online challenge: automatic detection of microaneurysms in digital color fundus photographs," *IEEE Trans. Med. Imaging*, vol. 29, no. 1, pp. 185–195, 2009.
[42] J. Cuadros and G. Bresnick, "EyePACS: an adaptable telemedicine system for diabetic retinopathy screening," *J. Diabetes Sci. Technol.*, vol. 3, no. 3, pp. 509–516, 2009.
[43] H. Mahdi, N. EL ABBADI, and H. RUSTUM, "SINGLE IMAGE DE-HAZING THROUGH IMPROVED DARK CHANNEL PRIOR AND ATMOSPHERIC LIGHT ESTIMATION.," *J. Theor. Appl. Inf. Technol.*, vol. 95, no. 15, 2017.
[44] N. el Abbadi, H. Mahdi, and H. Rustum, "Single image haze removal via accurate atmosphere light," *Int. J. Appl. Eng. Res.*, vol. 12, no. 19, pp. 9149–9158, 2017.
[45] M. Zhou, K. Jin, S. Wang, J. Ye, and D. Qian, "Color retinal image enhancement based on luminosity and contrast adjustment," *IEEE Trans. Biomed. Eng.*, vol. 65, no. 3, pp. 521–527, 2017.
[46] P. Dai, H. Sheng, J. Zhang, L. Li, J. Wu, and M. Fan, "Retinal fundus image enhancement using

the normalized convolution and noise removing," *Int. J. Biomed. Imaging*, vol. 2016, 2016.

[47] G. Palanisamy, P. Ponnusamy, and V. P. Gopi, "An adaptive enhancement method for low contrast color retinal images based on strucural similarity," in *2018 International Conference on Circuits and Systems in Digital Enterprise Technology (ICCSDET)*, 2018, pp. 1–4.

[48] Q. You, C. Wan, J. Sun, J. Shen, H. Ye, and Q. Yu, "Fundus image enhancement method based on CycleGAN," in *2019 41st annual international conference of the IEEE engineering in medicine and biology society (EMBC)*, 2019, pp. 4500–4503.

[49] Y. Luo *et al.*, "Dehaze of cataractous retinal images using an unpaired generative adversarial network," *IEEE J. Biomed. Heal. Informatics*, vol. 24, no. 12, pp. 3374–3383, 2020.

[50] K. Aurangzeb, S. Aslam, M. Alhussein, R. A. Naqvi, M. Arsalan, and S. I. Haider, "Contrast Enhancement of Fundus Images by Employing Modified PSO for Improving the Performance of Deep Learning Models," *IEEE Access*, vol. 9, pp. 47930–47945, 2021.

[51] J. Wang, Y.-J. Li, and K.-F. Yang, "Retinal fundus image enhancement with image decomposition and visual adaptation," *Comput. Biol. Med.*, vol. 128, p. 104116, 2021.

[52] Alghamdi, H. S. & Tang, H. L. & Waheeb, S. A. & Peto, T., "Automatic Optic Disc Abnormality Detection in Fundus Images: A Deep Learning Approach", *Ophthalmic Medical Image Analysis International Workshop* 3(2016), p.17-24. doi: https://doi.org/10.17077/omia.1042

[53] X. Wu, B. Dai, and W. Bu, "Optic disc localization using directional models," *IEEE Trans. Image Process.*, vol. 25, no. 9, pp. 4433–4442, 2016.

[54] P. Xu, C. Wan, J. Cheng, D. Niu, and J. Liu, "Optic disc detection via deep learning in fundus images," in *Fetal, infant and ophthalmic medical image analysis*, Springer, 2017, pp. 134–141.

[55] M. E. Martinez-Perez, N. Witt, K. H. Parker, A. D. Hughes, and S. A. M. Thom, "Automatic optic disc detection in colour fundus images by means of multispectral analysis and information content," *PeerJ*, vol. 7, p. e7119, 2019.

[56] K. Hu *et al.*, "Retinal vessel segmentation of color fundus images using multiscale convolutional neural network with an improved cross-entropy loss function," *Neurocomputing*, vol. 309, pp. 179–191, 2018.

[57] Z. Gu *et al.*, "Ce-net: Context encoder network for 2d medical image segmentation," *IEEE Trans. Med. Imaging*, vol. 38, no. 10, pp. 2281–2292, 2019.

[58] Q. Jin, Z. Meng, T. D. Pham, Q. Chen, L. Wei, and R. Su, "DUNet: A deformable network for retinal vessel segmentation," *Knowledge-Based Syst.*, vol. 178, pp. 149–162, 2019.

[59] M. A. U. Khan *et al.*, "A Scale Normalized Generalized LoG Detector Approach for Retinal Vessel Segmentation," *IEEE Access*, vol. 9, pp. 44442–44452, 2021.

[60] M. Abdullah, M. M. Fraz, and S. A. Barman, "Localization and segmentation of optic disc in retinal images using circular Hough transform and grow-cut algorithm," *PeerJ*, vol. 4, p. e2003, 2016.

[61] M. N. Zahoor and M. M. Fraz, "Fast optic disc segmentation in retina using polar transform," *IEEE Access*, vol. 5, pp. 12293–12300, 2017.

[62] R. G. Ramani and J. J. Shanthamalar, "Improved image processing techniques for optic disc segmentation in retinal fundus images," *Biomed. Signal Process. Control*, vol. 58, p. 101832, 2020.

[63] C. Yang, M. Lu, Y. Duan, and B. Liu, "An efficient optic cup segmentation method decreasing the influences of blood vessels," *Biomed. Eng. Online*, vol. 17, no. 1, pp. 1–15, 2018.

[64] J. Pruthi, K. Khanna, and S. Arora, "Optic Cup segmentation from retinal fundus images using Glowworm Swarm Optimization for glaucoma detection," *Biomed. Signal Process. Control*, vol. 60, p. 102004, 2020.

[65] P. H. Prastyo, A. S. Sumi, and A. Nuraini, "Optic Cup Segmentation using U-Net Architecture on Retinal Fundus Image," *JITCE (Journal Inf. Technol. Comput. Eng.*, vol. 4, no. 02, pp. 105–109, 2020.

[66] L. C. Rodrigues and M. Marengoni, "Segmentation of optic disc and blood vessels in retinal images using wavelets, mathematical morphology and Hessian-based multi-scale filtering," *Biomed. Signal Process. Control*, vol. 36, pp. 39–49, 2017.

[67] G. Y. Kim, S. H. Lee, and S. M. Kim, "Automated segmentation and quantitative analysis of optic disc and fovea in fundus images," *Multimed. Tools Appl.*, pp. 1–16, 2021.

[68] E. J. Carmona and J. M. Molina-Casado, "Simultaneous segmentation of the optic disc and fovea

in retinal images using evolutionary algorithms," *Neural Comput. Appl.*, vol. 33, no. 6, pp. 1903–1921, 2021.

[69] S. M. Shankaranarayana, K. Ram, K. Mitra, and M. Sivaprakasam, "Joint optic disc and cup segmentation using fully convolutional and adversarial networks," in *Fetal, infant and ophthalmic medical image analysis*, Springer, 2017, pp. 168–176.

[70] M. Tabassum *et al.*, "CDED-Net: Joint segmentation of optic disc and optic cup for glaucoma screening," *IEEE Access*, vol. 8, pp. 102733–102747, 2020.

[71] B. Liu, D. Pan, and H. Song, "Joint optic disc and cup segmentation based on densely connected depthwise separable convolution deep network," *BMC Med. Imaging*, vol. 21, no. 1, pp. 1–12, 2021.

[72] A. Sevastopolsky, "Optic disc and cup segmentation methods for glaucoma detection with modification of U-Net convolutional neural network," *Pattern Recognit. Image Anal.*, vol. 27, no. 3, pp. 618–624, 2017.

[73] T. Nazir, A. Irtaza, and V. Starovoitov, "Optic Disc and Optic Cup Segmentation for Glaucoma Detection from Blur Retinal Images Using Improved Mask-RCNN," *Int. J. Opt.*, vol. 2021, 2021.

[74] J. Ayub *et al.*, "Glaucoma detection through optic disc and cup segmentation using K-mean clustering," in *2016 international conference on computing, electronic and electrical engineering (ICE Cube)*, 2016, pp. 143–147.

[75] J. Zilly, J. M. Buhmann, and D. Mahapatra, "Glaucoma detection using entropy sampling and ensemble learning for automatic optic cup and disc segmentation," *Comput. Med. Imaging Graph.*, vol. 55, pp. 28–41, 2017.

[76] N. A. Mohamed, M. A. Zulkifley, W. M. D. W. Zaki, and A. Hussain, "An automated glaucoma screening system using cup-to-disc ratio via Simple Linear Iterative Clustering superpixel approach," *Biomed. Signal Process. Control*, vol. 53, p. 101454, 2019.

[77] R. Ali *et al.*, "Optic Disc and Cup Segmentation Through Fuzzy Broad Learning System for Glaucoma Screening," *IEEE Trans. Ind. Informatics*, 2020.

[78] R. Imtiaz, T. M. Khan, S. S. Naqvi, M. Arsalan, and S. J. Nawaz, "Screening of Glaucoma disease from retinal vessel images using semantic segmentation," *Comput. Electr. Eng.*, vol. 91, p. 107036, 2021.

[79] A. Singh, M. K. Dutta, M. ParthaSarathi, V. Uher, and R. Burget, "Image processing based automatic diagnosis of glaucoma using wavelet features of segmented optic disc from fundus image," *Comput. Methods Programs Biomed.*, vol. 124, pp. 108–120, 2016.

[80] N. Kavya and K. V Padmaja, "Glaucoma detection using texture features extraction," in *2017 51st Asilomar Conference on Signals, Systems, and Computers*, 2017, pp. 1471–1475.

[81] A. A. G. Elseid and A. O. Hamza, "Glaucoma detection based on shape features and SMOTE algorithm," *Digit. Image Process.*, vol. 10, no. 10, pp. 192–196, 2018.

[82] L. Abdel-Hamid, "Glaucoma detection from retinal images using statistical and textural wavelet features," *J. Digit. Imaging*, vol. 33, no. 1, pp. 151–158, 2020.

[83] M. M. Sathik, A. Padma, and M. Sivajothi, "Glaucoma Detection Using Little Wood Paley Decomposition On Local Derivative Structure Of Fundus Images," *Eur. J. Mol. Clin. Med.*, vol. 7, no. 10, pp. 2988–2998, 2021.

[84] Z. Li, Y. He, S. Keel, W. Meng, R. T. Chang, and M. He, "Efficacy of a deep learning system for detecting glaucomatous optic neuropathy based on color fundus photographs," *Ophthalmology*, vol. 125, no. 8, pp. 1199–1206, 2018.

[85] H. Fu *et al.*, "Disc-aware ensemble network for glaucoma screening from fundus image," *IEEE Trans. Med. Imaging*, vol. 37, no. 11, pp. 2493–2501, 2018.

[86] M. Christopher *et al.*, "Performance of deep learning architectures and transfer learning for detecting glaucomatous optic neuropathy in fundus photographs," *Sci. Rep.*, vol. 8, no. 1, pp. 1–13, 2018.

[87] U. Raghavendra, H. Fujita, S. V Bhandary, A. Gudigar, J. H. Tan, and U. R. Acharya, "Deep convolution neural network for accurate diagnosis of glaucoma using digital fundus images," *Inf. Sci. (Ny).*, vol. 441, pp. 41–49, 2018.

[88] S. Serte and A. Serener, "Graph-based saliency and ensembles of convolutional neural networks for glaucoma detection," *IET Image Process.*

[89] R. Hemelings *et al.*, "Accurate prediction of glaucoma from colour fundus images with a

convolutional neural network that relies on active and transfer learning," *Acta Ophthalmol.*, vol. 98, no. 1, pp. e94–e100, 2020.
[90] R. C. Joshi, M. K. Dutta, P. Sikora, and M. Kiac, "Efficient Convolutional Neural Network Based Optic Disc Analysis Using Digital Fundus Images," in *2020 43rd International Conference on Telecommunications and Signal Processing (TSP)*, 2020, pp. 533–536.
[91] M. Alghamdi and M. Abdel-Mottaleb, "A Comparative Study of Deep Learning Models for Diagnosing Glaucoma from Fundus Images," *IEEE Access*, vol. 9, pp. 23894–23906, 2021.
[92] Y. Bao *et al.*, "Self-Adaptive Transfer Learning for Multicenter Glaucoma Classification in Fundus Retina Images," *arXiv Prepr. arXiv2105.03068*, 2021.
[93] P. K. Chaudhary and R. B. Pachori, "Automatic diagnosis of glaucoma using two-dimensional fourier-bessel series expansion based empirical wavelet transform," *Biomed. Signal Process. Control*, vol. 64, p. 102237, 2021.